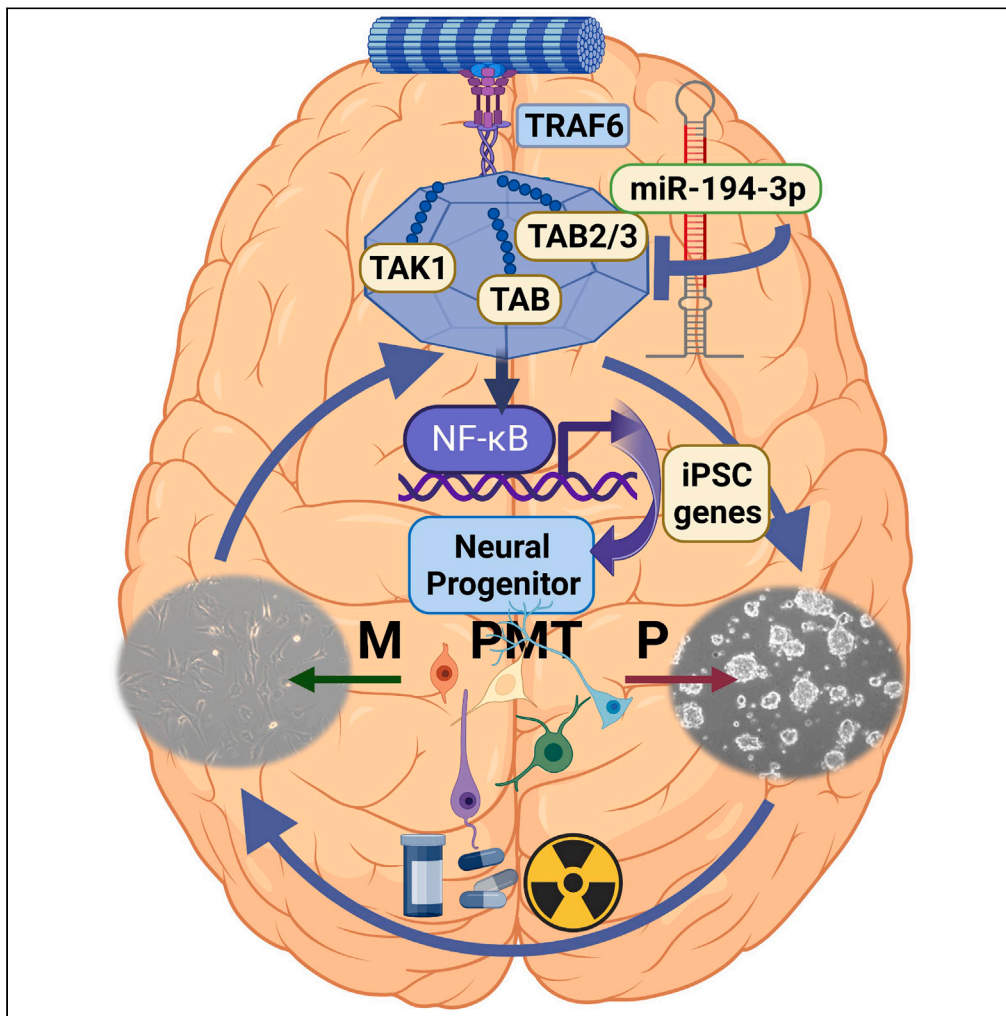


Article

miRNA-194-3p represses NF-κB in gliomas to attenuate iPSC genes and proneural to mesenchymal transition



John Ryan Jacob,
Rajbir Singh, Masa
Okamoto, Arnab
Chakravarti,
Kamalakaran
Palanichamy

kamalakaran.palanichamy@
osumc.edu

Highlights

GSCs suppress miR-194-3p
to promote TAB2
mediated NF-κB activation

GBMs utilize miR-194-3p to
transcriptionally regulate
iPSC factors and tumor
subtypes

Disrupting miR-194-3p/
TAB2/NF-κB signaling axis
inhibits PMT

Genetic ablation of miR-
194-3p/TAB2/NF-κB axis
diminishes tumor
heterogeneity

Jacob et al., iScience 27,
108650
January 19, 2024 © 2023 The
Authors.
[https://doi.org/10.1016/
j.isci.2023.108650](https://doi.org/10.1016/j.isci.2023.108650)

Article

miRNA-194-3p represses NF- κ B in gliomas to attenuate iPSC genes and proneural to mesenchymal transitionJohn Ryan Jacob,¹ Rajbir Singh,¹ Masa Okamoto,^{1,2} Arnab Chakravarti,^{1,3} and Kamalakannan Palanichamy^{1,3,4,*}

SUMMARY

Severe tumor heterogeneity drives the aggressive and treatment refractory nature of glioblastomas (GBMs). While limiting GBM heterogeneity offers promising therapeutic potential, the underlying mechanisms that regulate GBM plasticity remain poorly understood. We utilized 14 patient-derived and four commercially available cell lines to uncover miR-194-3p as a key epigenetic determinant of stemness and transcriptional subtype in GBM. We demonstrate that miR-194-3p degrades TAB2, an important mediator of NF- κ B activity, decreasing NF- κ B transcriptional activity. The loss in NF- κ B activity following miR-194-3p overexpression or TAB2 silencing decreased expression of induced pluripotent stem cell (iPSC) genes, inhibited the oncogenic IL-6/STAT3 signaling axis, suppressed the mesenchymal transcriptional subtype in relation to the proneural subtype, and induced differentiation from the glioma stem cell (GSC) to monolayer (ML) phenotype. miR-194-3p/TAB2/NF- κ B signaling axis acts as an epigenetic switch that regulates GBM plasticity and targeting this signaling axis represents a potential strategy to limit transcriptional heterogeneity in GBMs.

INTRODUCTION

Intratumor heterogeneity is one of the major hallmarks of glioblastoma (GBM).¹ In GBMs, glioma stem cells (GSCs) drive treatment resistance and the aggressive nature of the tumors.² It has been shown that GSCs are not clonal entities but rather exist in a plastic state shaped by microenvironmental niches.³ GSCs harbor the treatment resistance compartment of GBM tumors and are composed of cells capable of differentiation to different neural lineages.² We hypothesize that targeting this inherent cell plasticity will emerge as a treatment strategy for better therapeutic outcomes while eradicating tumor heterogeneity. In this work, we modeled genetically identical undifferentiated neurosphere and differentiated adherent phenotypes representing the extreme ends of plasticity to decipher the epigenetic targets mediating phenotype transition and tumor heterogeneity. We show that *in situ* this differentiation phenomenon is controlled by transcription factors including nuclear factor κ B (NF- κ B) activation followed by activation of induced pluripotency stem cell (iPSC) genes.

Previous studies have reported that NF- κ B activation encodes more aggressive GSC phenotype. Activation of NF- κ B occurs in solid tumors to promote epithelial to mesenchymal transition (EMT), invasion, angiogenesis, and metastasis.^{4–6} Current treatment regimens chemotherapy and/or radiotherapy activate NF- κ B resulting in alterations to critical features involving proliferation, inflammation, innate and adaptive immunity, and tumor development.⁷ Abnormally high activation of NF- κ B signaling is strongly correlated with acquired temozolomide (TMZ) resistance and poor prognosis in GBM.⁸ Activation of NF- κ B promotes mesenchymal *trans*-differentiation and radio-resistance in GSC.⁹ Patient-derived GSCs undergo differentiation with a subset of cells displaying mesenchymal signature, exhibiting resistance to radiation and targeted therapies resulting in aggressive tumor formation and NF- κ B activation.¹⁰ NF- κ B signaling was identified as a key mediator of mesenchymal GSC exosome induced angiogenesis.¹¹ The invasive phenotype of GBM is orchestrated by the transcription factor NF- κ B which, via metalloproteinase, regulates fibronectin processing.¹²

Despite significant advances in understanding of NF- κ B pathway, our ability to effectively block key targets in this pathway clinically for cancer therapy remains limited due to on-target effects in normal tissues.¹³ Targeting pathogenic NF- κ B signaling in cancer, while preserving the multiple physiological functions of NF- κ B is crucial.¹⁴ Thus, it is essential to decipher NF- κ B pleiotropic biological function and pathological contribution to develop appropriate therapeutic against cancer. One of the strategies is to use epigenetic targets which are emerging modulators in the transcription factor arena. Through this work, we demonstrate that suppression of miR-194-3p is required

¹Department of Radiation Oncology, The Ohio State University College of Medicine and Comprehensive Cancer Center, Columbus, OH 43210, USA

²Department of Radiation Oncology, Gunma University Graduate School of Medicine, Gunma 371-8511, Japan

³Senior author

⁴Lead contact

*Correspondence: kamalakannan.palanichamy@osumc.edu
<https://doi.org/10.1016/j.isci.2023.108650>



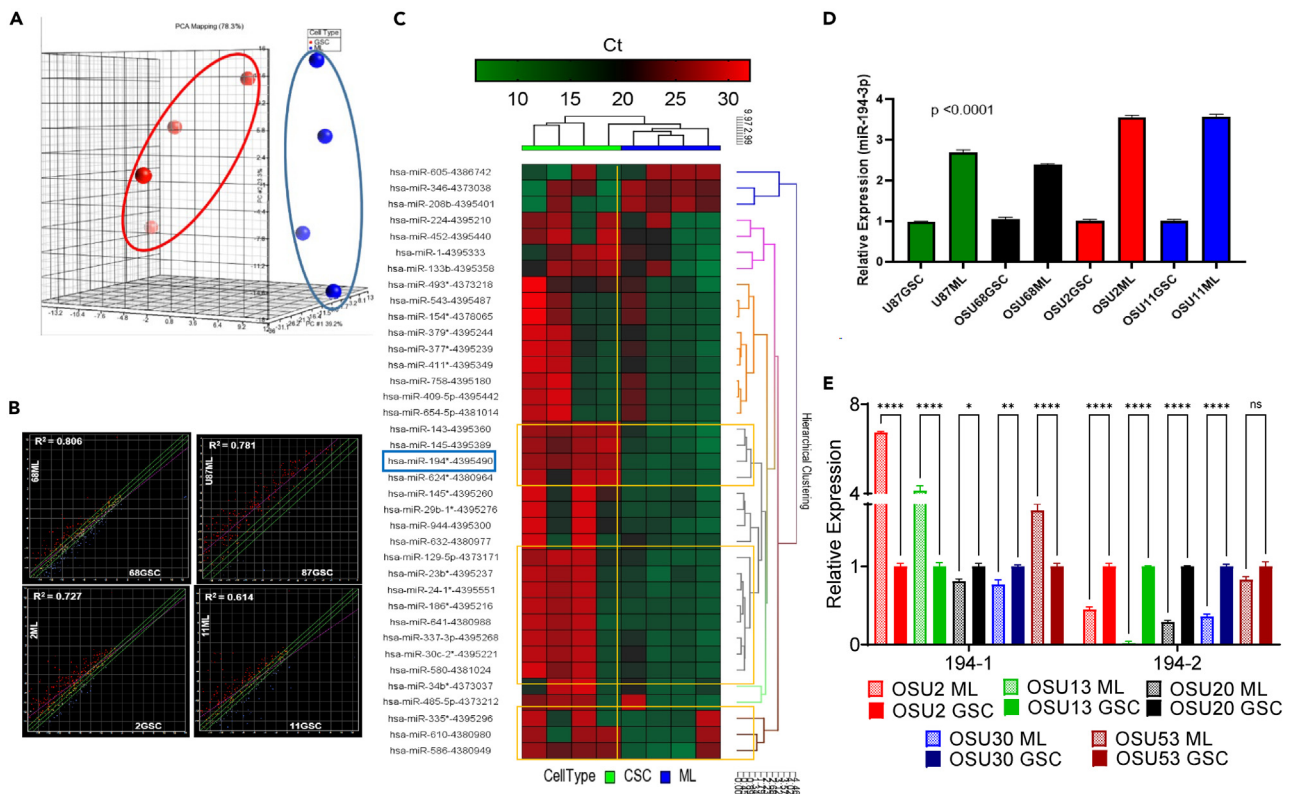


Figure 1. miRNA expression profiling and expression levels of miR-194-3p in ML and GSC counterparts, and pre-miR-194-1 & 194-2 expression levels
 (A) Principal component analysis of miRNA expression profiling. ML and GSC cell lines are demarcated by blue and red respectively.
 (B) Correlation plots of miRNA expression levels in matched pair ML and GSC cell lines.
 (C) Heatmap representing the most differentially regulated miRNA between ML and GSC cell lines. The yellow boxes indicate the miRNAs upregulated in the ML cell lines compared to the GSC cell lines. miR-194-3p is marked by a blue box.
 (D) miR-194-3p expression levels in ML and GSC cell lines. Data are shown as mean \pm SEM. Statistical significance was tested using two-tailed unpaired t-test. All comparisons between matched pair ML and GSC cell lines demonstrated a p value less than 0.0001.
 (E) The expression levels of the pre-miRNA 194-1 and 194-2 in paired ML and GSC cell lines. Data are shown as mean \pm SEM. Statistical significance was tested using two-tailed unpaired t-test. ns not significant; *p < 0.05; **p < 0.01; ***p < 0.001; ****p < 0.0001.

to sustain NF- κ B activation to enhance iPSC gene expression and regulating proneural to mesenchymal transition (PMT) and tumor heterogeneity.

RESULTS

miRNA profiling identifies miRNA-194-3p as a differentially regulated miRNA in paired adherent monolayer (ML) and glioma stem cells (GSC) enriched from tumor biopsies

We started our investigation into the epigenetic determinants of GBM stemness by performing microRNA (miRNA) screens on matched pair monolayer (ML) and GSC cultures. In comparison to MLs, GSCs possess an enhanced expression of induced pluripotent stem cell (iPSC) genes and form tumors that more closely resemble GBM biology.^{2,15,16} While previous studies profiled the differences in miRNA expression across either MLs or GSCs,^{17–19} miRNA profiles between matched ML and GSCs remains unexplored. We observed a clear separation in the miRNA profiles between matched pair MLs and GSCs derived from the patient derived OSU2, OSU11 and OSU68 and U87 cell lines (Figure 1A). They exhibited several differentially regulated miRNAs as indicated by the correlation plot between GSC and ML within the same tumor suggesting cellular subtype heterogeneity ($R^2 = 0.61$ to 0.80) (Figure 1B). The data were normalized by global normalization algorithm and U6 calibrator expression levels across all cell lines were very close within ± 0.1 in seven out of eight cell lines and ± 0.3 in OSU2 (Table S1). By applying rigorous statistical criteria on the matched GSC and ML miRNA data, we identified the miR-143/miR-145 cluster along with miR-194-3p as differentially regulated across all ML/GSC pairs tested (Figure 1C). The miR-143 and miR-145 form a bicistronic cluster in chromosome 5q33.1 and are reported to promote cancer cell differentiation.²⁰ Based on the number of published materials on miR-143/145 cluster connecting to SOX2 which is implicated in stem cell genotype, we focused on the target miR-194-3p. The expression levels of miR-194-3p were validated to be upregulated in the differentiated ML phenotype in all four ML/GSC pairs tested (Figure 1D).

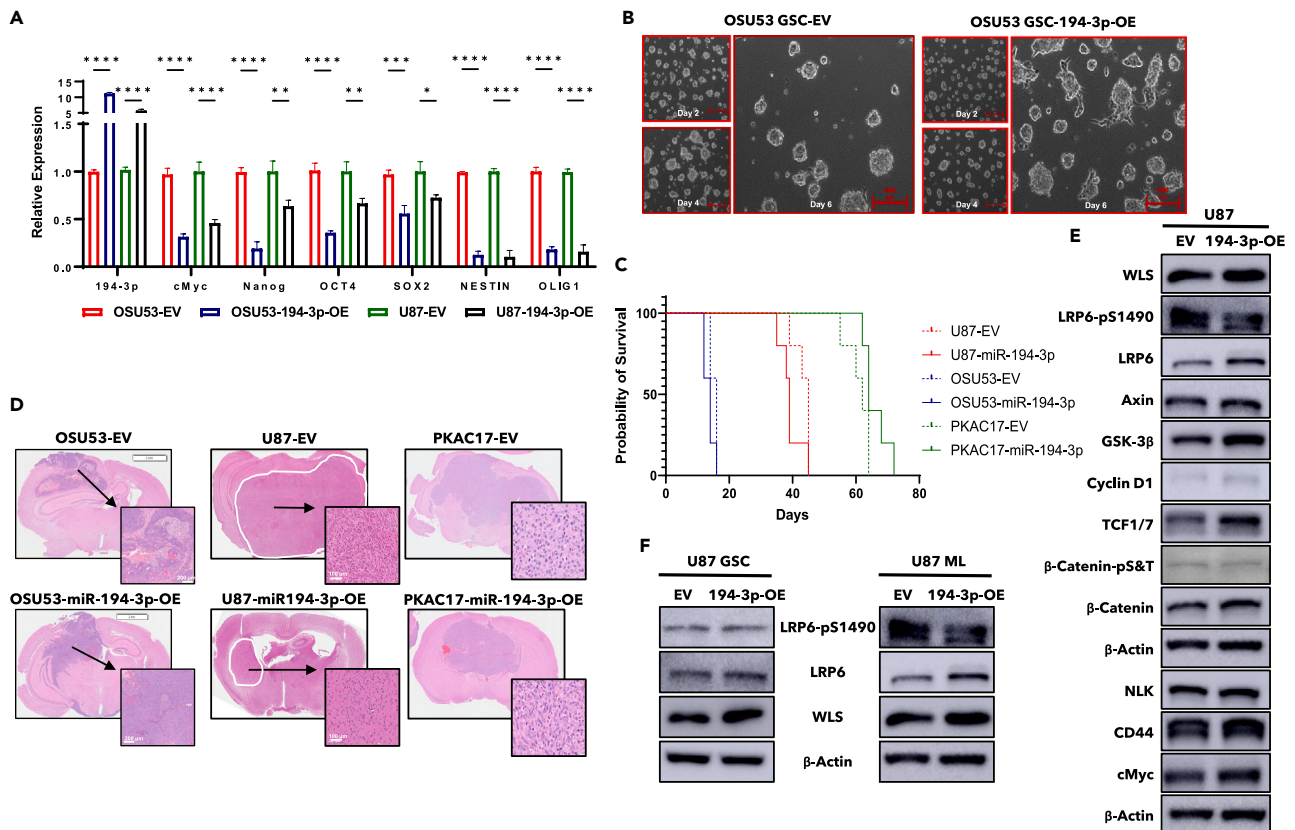


Figure 2. Expression levels of induced pluripotent stem cell (iPSC) genes, lineage markers, effect of miR-194-3p alterations on neurosphere formation, survival, and H&E staining of coronal sections of intracranial tumors obtained from isogenic miR-194-3p cells, and WLS pathway signaling cascades
 (A) Lineage and iPSC marker expression levels in miR-194-3p isogenic cell lines. Data are shown as mean \pm SEM. Statistical significance was tested using two-tailed unpaired t-test.
 (B) Representative images demonstrating the phenotype of OSU53GSC-EV and OSU53GSC-194-3p-OE cells in GSC culture conditions.
 (C) Kaplan-Meier survival curves of nude mice bearing U87-, PKAC17- and OSU53-194-3p isogenic tumors. The p value was calculated using the two-sided log rank test.
 (D) H&E staining of the intracranial tumors formed from U87-, PKAC17- and OSU53-194-3p isogenic xenografts.
 (E) Western blot analysis of WNT signaling proteins in U87-EV and U87-194-3p-OE ML cells.
 (F) Activation level of LRP6 in U87-EV and U87-194-3p-OE cells grown under both ML and GSC culture conditions. ns not significant; *p < 0.05; **p < 0.01; ***p < 0.001; ****p < 0.0001.

miRNA-194-3p expression correlates with ML/GSC subtypes in GBM cells, and miRNA-194-3p overexpression decrease tumor burden

Two putative pairs of orthologous hairpin precursor structures are found in human (miR-194-1 (MI0000488) on chromosome 1 and miR-194-2 (MI0000732) on chromosome 11. miR-194-1 produces the miR-194-5p mature sequence, whereas miR-194-2 produces both miR-194-3p and miR-194-5p. The expression levels of 194-1 was found to be significantly downregulated in GSCs compared to the ML counterparts, whereas 194-2 expression levels were higher in GSCs compared to ML (Figure 1E). Though miR-194-2 expression levels were high in GSCs compared to ML, the mature miR-194-3p was lower in GSCs which could be due to alternate splicing of miRNAs as well as in the inhibitory effects of opposite strands that are not currently well understood and beyond the scope of the current work. The iPSC and other lineage relevant genes were significantly downregulated in miR-194-3p overexpression cell lines (Figure 2A). Isogenic miR-194-3p cells promoted the transformation from the floating GSC to adherent ML phenotype (Figure 2B). Similarly, miR-194-3p expression in ML cells prevented sphere forming ability to the GSC phenotype (Figure S1A). These characteristics shows the regulatory role of miR-194-3p in GSC differentiation and ML de-differentiation or sphere forming ability. To exclude the possibility of miR-194-5p interaction, we tested the expression levels of direct targets C21orf91 and TRIM23 in miR-194-3p isogenic cell lines (Figure S1B). Expression levels of both gene targets were not altered in miR-194-3p overexpression cells clearly eliminating the possibility of miR-194-5p involvement in this phenomenon. Tumor forming ability was evaluated by intracranial implantation of mesenchymal subtype OSU53, proneural subtype PKAC17 and U87 miR-194-3p isogenic cells. Two weeks after implantation nude mice bearing OSU53 cells developed severe neurological symptoms, whereas nude mice bearing U87 cells developed symptoms in four

weeks after implantation and PKAC17 cells developed symptoms 8 weeks after implantation (Figure 2C). We did not observe any statistically different survival benefit in nude mice bearing miR-194-3p isogenic cells in all the three cell lines tested. In mesenchymal OSU53 Hematoxylin and Eosin (H&E) staining demonstrated that miR-194-3p overexpression decreased tumor aggressiveness, indicated by a reduction in pseudopalisading and necrotic areas (Figure 2D). Additionally, tumors derived from miR-194-3p overexpression cells possessed a decrease in Nestin levels (Figure S4). We concluded that miR-194-3p expression influences tumor aggression and neuronal progenitor OSU53 *in vivo*. Of note, in proneural PKAC17, we did not see any pseudopalisading or necrotic areas which may be due to the nature of cell line.

miRNA-194-3p promotes the ML phenotype independent of the WNT/ β -catenin pathway and G-CIMP status

To predict the targets of miR-194-3p, we utilized the web interface for integrative analysis of miRNA target prediction and functional annotations (miRDB).^{21,22} Table S2 provides the top 25 predicted sites of miR-194-3p using the miRDB algorithm. TAB2 was predicted as one of the potential targets with a score of 95%. To cross check informatics, we used TargetScan database.²³ TargetScan predicted 6224 sites containing 4559 transcripts. However, a majority of confidently predicted targets may not be functional because both miRNA and mRNA may not be expressed in the same cell at the same time and at the same location and at the expression level sufficient to mediate regulation and consequential repression. Ideally, miRNA expression must exceed 1000 molecules per cell for detectable repression. We selected the top 50 transcripts listed in Table S3. After filtering the targets based on their expression and significance to the study, we investigated WLS and TAB2 based on their reported roles in regulating the stem cell phenotype. WLS is a WNT ligand that promotes stem cell developmental pathways by activating β -catenin.²⁴ TAB2, TGF-Beta Activated Kinase 1/MAP3K7 Binding Protein, encodes an activator of MAP3K7/TAK1, which is required for the activation of NF- κ B.²⁵ In addition, TAB2 regulates β -catenin transcription through the activation of the NLK kinase and consequent stabilization of the LEF1/TCF complex.²⁶ Given the important role of WNT signaling in stem cell maintenance, we hypothesized that miR-194-3p downregulates the WNT/ β -catenin pathway. However, miR-194-3p overexpression did not induce significant changes in the protein level of WLS or β -catenin (Figure 2E). While we observed an increase in the protein levels of LEF1/TCF, the protein levels of β -catenin-LEF1/TCF target proteins CD44 and c-Myc did not change (Figure 2E). To ascertain that these variations are not due to culturing conditions, we evaluated the expression levels of the pathway members in both ML and GSC culture conditions. In both cases, the overexpression of miR-194-3p did not change the level of WLS in the system (Figure 2F). Together, we conclude that miR-194-3p functions independently of the WNT/ β -catenin pathway.

It has been reported that IDH mutant G-CIMP-high subtype would be a predecessor to the G-CIMP-low subtype and CpG island methylator phenotype defines a distinct subgroup of glioma.^{27,28} Genetic alterations and epigenetic plasticity contributing to G-CIMP malignant evolution toward an IDH-wild-type and mesenchymal/stem cell-like GBM phenotype remain unexplored. The GSCs used in the study are IDH-wild-type grade IV tumor exhibiting enhanced tumorigenicity in GSC phenotype compared to ML phenotype. We questioned whether this shift occurs due to alterations in methylation epigenetic landscape. Accordingly, we wanted to check whether there is a shift in G-CIMP status defining markers in GSC and ML phenotype by analyzing the expression levels of markers such as DOCK5, FAS, HFE, LGALS3, MAL, RHOF, and SOWHA for their hyper- or hypo-methylation status. We also tested whether miR-194-3p shifts the methylation landscape by profiling the G-CIMP markers (Figure S1C), we observed downregulation of LGALS3, MAL, and SOWHA, while the rest DOCK5, FAS, HFE, and RHOF show only modest changes. This observation eliminates the possibility of shift from G-CIMP+ to G-CIMP- phenotype.

miRNA-194-3p suppresses NF- κ B activation by silencing TAB2 and TAB2 expression correlates with proneural (P)/mesenchymal (M) GSCs

Next, we investigated the role of the miR-194-3p target TAB2 in regulating the ML/GSC phenotypes. The higher expression of miR-194-3p in the ML phenotype is associated with a decreased expression of TAB2 and iPSC gene expression (Figures 3A–3C; Table S4). In support of the role of TAB2 in regulating the ML/GSC phenotype, we observed a decreased expression of TAB2 in LN229 cells, which are unable to form neurospheres under GSC culture conditions, in comparison to neurosphere forming cells U87 and A172 (Figure 3C). This suggests that miR-194-3p regulates the ML/GSC phenotypes by dictating TAB2 levels. Next, we determined the role of the TAB2 target NF- κ B in regulating the ML/GSC phenotypes. The basal expression levels of activated NF- κ B shows an inverse correlation with the TAB2 expression levels in GSC and ML counterparts (Figure 3D). Transfection with miR-194-3p mimic and inhibitor was sufficient to alter NF- κ B activation (Figure 3E). Mesenchymal GSCs possessed a higher expression of TAB2 compared to proneural GSCs (Figure 3F). We cross-examined the association of TAB2 with GSC subtypes by analyzing the dataset at gene expression omnibus (GSE4916229) comprising mesenchymal and proneural GSCs. This confirmed that TAB2 expression aligns with the mesenchymal subtype (Figure S2). Induced expression of miR-194-3p in mesenchymal OSU53 GSCs exhibited a shift to the P phenotype (Figure 3G), suggesting that miR-194-3p:TAB2 regulation mediates proneural to mesenchymal transition (PMT).

miRNA-194-3p-TAB2 binding validation

We cloned sequences representing the TAB2 3' UTR with intact and mismatched miR-194-3p binding site into a luciferase reporter system (Figure 4A). The transfection of the luciferase reporter plasmids was followed by the addition of miR-194-3p mimic and inhibitor in U87 cells. The luciferase reporter fused to the intact TAB2 UTR sequence showed a marked decrease following the addition of miR-194-3p mimic that was rescued by the concurrent addition of miR-194-3p inhibitor (Figure 4B). This effect was not observed with the luciferase reporter containing the mismatched TAB2 UTR sequence (Figure 4B). Similarly, we added the luciferase reporter plasmids to the U87-EV and U87-194-3p-OE cell lines to determine whether the forced expression of endogenous miR-194-3p demonstrated the same effect. As expected, the U87-194-

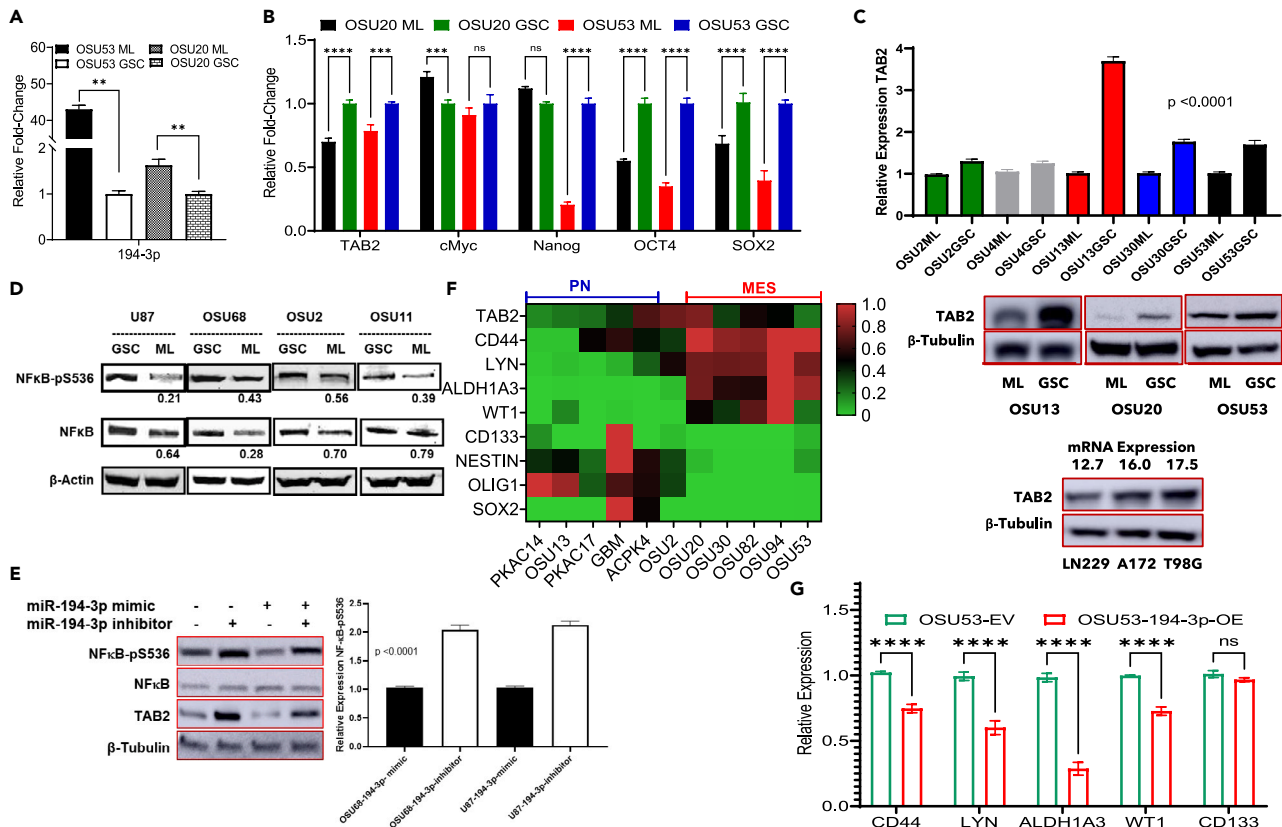


Figure 3. miR-194-3p, TAB2 and iPSC gene expression in GSC vs. ML counterparts, miR-194-3p modulates NF-κB activation in GSC vs. ML matched pairs, TAB2 expression correlates with P and M subtype

(A) The expression levels of miR-194-3p in matched pair ML and GSC cell lines. Data are shown as mean ± SEM. Statistical significance was tested using two-tailed unpaired t-test.

(B) Relative expression levels of TAB2 and iPSC markers in matched GSC and ML pairs. Data are shown as mean ± SEM. Statistical significance was tested using two-tailed unpaired t-test.

(C) Top: Quantification of TAB2 protein levels in panel of ML and GSC cell lines. Data are shown as mean ± SEM. Statistical significance was tested using two-tailed unpaired t-test. Middle: TAB2 protein levels in OSU13, OSU20 and OSU53 matched pair ML and GSC cell lines. Bottom: TAB2 protein levels in commercially available GBM cell lines; Corresponding mRNA expression are represented above images.

(D) Western blot analysis of NF-κB activation in matched pair ML and GSC cell lines.

(E) NF-κB activation following the transfection of 100 nM miR-194-3p mimic and inhibitor in U87 ML and OSU68 ML cells.

(F) The heatmap represents the relative expression of TAB2, mesenchymal and proneural markers in the GSC cell lines. Data is row-normalized data.

(G) Expression levels of proneural and mesenchymal markers in miR-194-3p isogenic cells. Data are shown as mean ± SEM. Statistical significance was tested using two-tailed unpaired t-test. ns not significant; **p < 0.01; ***p < 0.001; ****p < 0.0001.

3p-OE cell line demonstrated a significant decrease in the luciferase fused to the intact TAB2 UTR that was partially rescued by the addition of miR-194-3p inhibitor (Figure 4C). This was not observed with the mismatched TAB2 UTR sequence (Figure 4C). Together, this suggests miR-194-3p directly targets TAB2.

miR-194-3p and TAB2 regulation

To determine whether TAB2 silencing produces the same phenotype as miR-194-3p OE cells, we generated stable TAB2 knockdown cell lines (Figures 4D and 4E). TAB2 silencing downregulated the iPSC genes recapitulating the same features of miR-194-3p-OE cells (Figure 4E). Isogenic TAB2 and miR-194-3p-OE similarly altered the IL6/STAT3/NF-κB signaling cascade (Figure 5A). Silencing TAB2 blocked the transition from the ML to GSC phenotype under neurosphere culturing conditions (Figure S3). TAB2 silencing in mesenchymal OSU53 GSCs initiated a transition to the adherent phenotype (Figures 5B and 5C), like miR-194-3p overexpression. miR-194-3p and TAB2 isogenic cells possessed a decrease in NF-κB activity, measured by promoter binding (Figures 5D and 5E). Additionally, TAB2 knockdown cells exhibited a downregulation of iPSC genes both at transcriptional and translational levels (Figures 5F and 5G). We conclude that miR-194-3p induction or TAB2 inhibition blocks PMT, as validated in both U87ML and OSU53GSC cell lines.

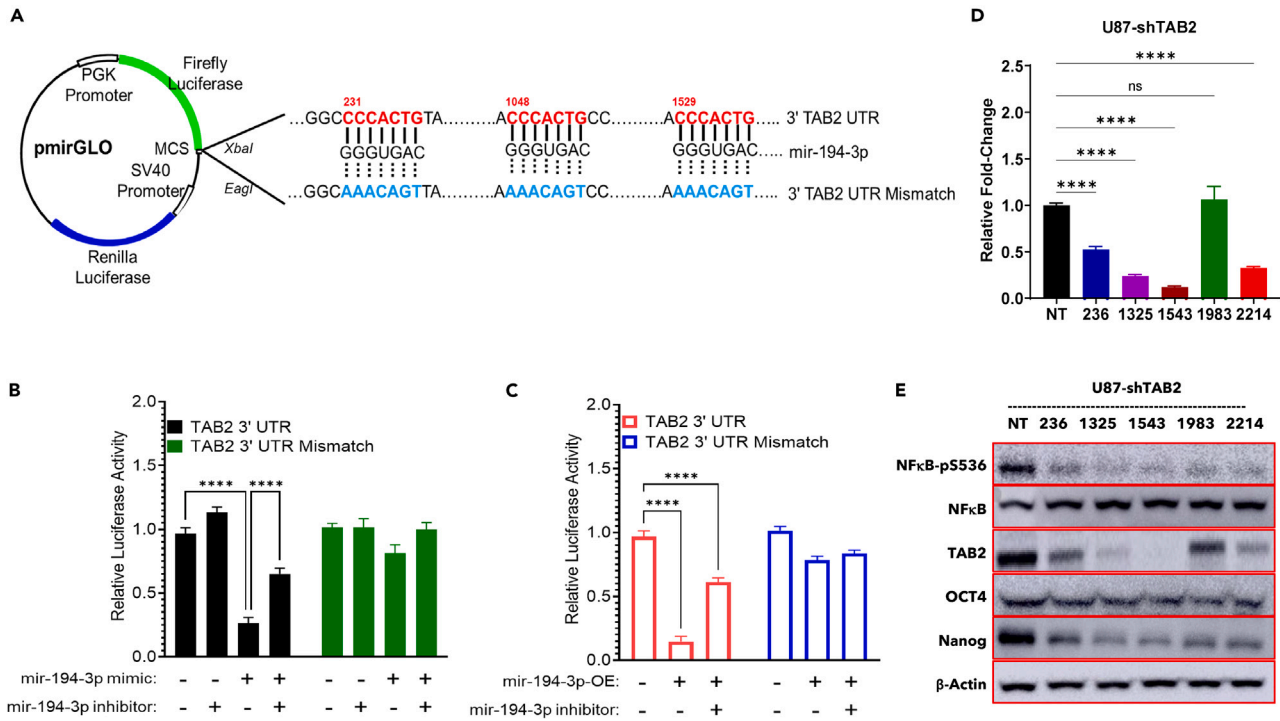


Figure 4. Luciferase reporter assay confirming inhibition of TAB2 by miR-194-3p, expression level of TAB2, NF- κ B, and iPSC markers in U87-TAB2 isogenic cells

(A) Schematic of the TAB2 3' UTR miRNA reporter system. Sequences representing the TAB2 3' UTR and a mismatched control were cloned into the reporter system downstream of the firefly luciferase protein (PGK). The Renilla luciferase protein was driven off a second promoter (SV40) and used as a control for transfection efficiency.

(B) The miRNA reporter vectors were transfected in U87 cells for 24 h before treating with 100 nM miR-194-3p mimic or inhibitor. Activity is represented by the amount of firefly luciferase normalized to the amount of Renilla luciferase. Data are shown as mean \pm SEM. Statistical significance was tested using two-way ANOVA (DF = 16).

(C) U87-EV and U87-194-3p-OE were transfected using the same conditions as B. Data are shown as mean \pm SEM. Statistical significance was tested using two-way ANOVA (DF = 12).

(D) Relative mRNA expression of TAB2 in U87 cells transfected with shTAB2.

(E) Relative TAB2, NF- κ B, and iPSC marker expression levels in TAB2 isogenic cell lines. ns not significant; ****p < 0.0001.

miRNA-194-3p modulate IL6/STAT3 signaling axis

Mesenchymal stem cells secrete interleukin 6 (IL6) to activate STAT3 and promote tumor growth and survival.^{30,31} Furthermore, inhibiting IL6-STAT3 signaling axis has been shown to inhibit proneural to mesenchymal transition.^{32,33} Extracellular vesicles utilize NF- κ B/STAT3 signaling axis to promote more aggressive mesenchymal phenotype.³⁴ The combined inhibition of both NF- κ B and STAT3 significantly increased the survival of mice bearing intracranial xenografts.³⁵ Therefore, we tested whether miR-194-3p/TAB2 modulation inhibits IL6/STAT3 pathway. In addition to NF- κ B, IL6/STAT3 signaling axis is also significantly downregulated (Figure 5A). Cytokines have been demonstrated to exacerbate the toxic effects of chemotherapy and affect drug metabolism. GSCs express IL6 receptors.³¹ Perturbing IL6 attenuates signal transducers and activators of transcription 3 (STAT3) activation and induces apoptosis indicating that STAT3 is a downstream mediator of IL6. Further, elevated levels of IL6 ligand and receptor expression are associated with poor survival outcome. The TAB2 or miR-194-3p can modulate "NF- κ B-IL6-STAT3" signaling axis and can provide a better prognosis.

Proof of concept: Decoupling heterogeneity and enriching P and M subtype from tumor biopsies

Growth factor defined serum free culture condition enriched GSC phenotype while serum condition alone enriches ML differentiated adherent phenotype from fresh tumor biopsies. In all the three tumor biopsies tested, both neurosphere (GSC) and adherent (ML) subtypes upon orthotopic implantation recapitulated aggressive nature of GBM exhibiting all histological hallmarks (Figure 6A). The tumor burden varies from cell line to cell line, but mouse bearing neurosphere phenotype produced tumor burden earlier than adherent phenotype while both developed pathologically similar tumors which can only be distinguished by immunostaining of appropriate markers (Figure 6B). The M subtype OSU53 and PKAC6 formed robust tumors crossing the midline with extensive angiogenesis, whereas P subtype PKAC14 formed diffuse and infiltrative tumors distributed all over the brain. Within the same tumor the GSC subtype was more tumorigenic than the ML

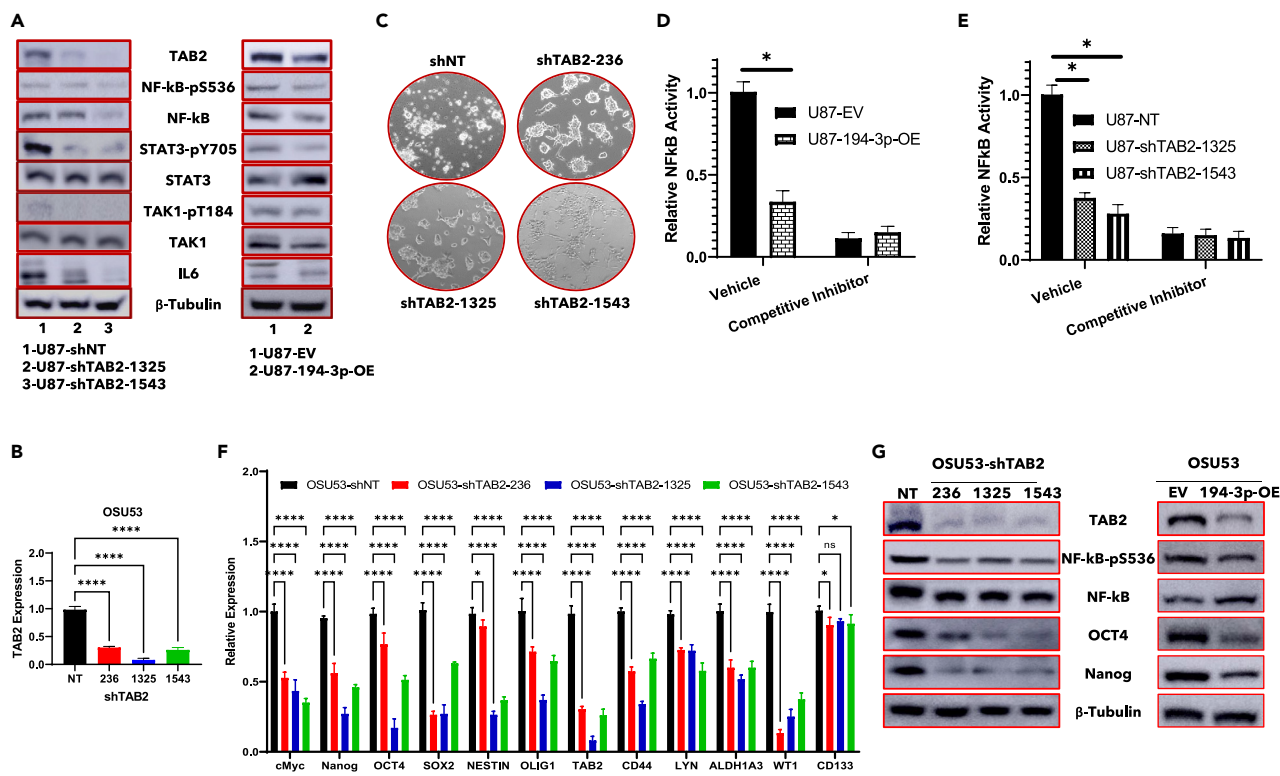


Figure 5. TAB2 silencing transforms GSC/P phenotype by downregulating NF-κB and iPSC genes promoting adherent/M phenotype

(A) Western blot analysis of the indicated proteins in U87-shTAB2 and U87-miR-194-3p isogenic cells. (B) TAB2 expression levels in OSU53-shTAB2 cell lines. Data are shown as mean \pm SEM. Statistical significance was tested using two-tailed unpaired t-test. (C) Microscopic image showing the morphological features of isogenic shTAB2 cells. (D and E) Relative NF-κB activity in TAB2 and miR-194-3p isogenic cells \pm competitive inhibitor measured using the NF-κB p65 Transcription Factor Assay Kit. Data are shown as mean \pm SEM. Statistical significance was tested using two-tailed unpaired t-test. (F) Expression levels of P/M and iPSC marker in isogenic OSU53-shTAB2 cells. Data are shown as mean \pm SEM. Statistical significance was tested using two-tailed unpaired t-test. (G) Western blot analysis of TAB2, NF-κB, and iPSC markers in OSU53-shTAB2 and OSU53-miR-194-3p isogenic cells. ns not significant; *p < 0.05; **p < 0.01; ***p < 0.001; ****p < 0.0001.

counterparts. The survival difference in GSC and ML in P subtype was higher than M subtype suggesting the differential regulation of time to tumor formation in these subtypes. OSU53GSC switched to adherent phenotype when miR-194-3p was overexpressed and blocked the PMT switch. ALDH1A3 expression separated the P vs. M subtype, miR-194-3p overexpression significantly decreased ALDH1A3 expressing cells within the tumor compared to EV controls, suggesting miR-194-3p retains the tumor in the P phenotype (Figure 6C). Immunohistochemical staining of OSU53 isogenic tumors demonstrated that miR-194-3p overexpression and TAB2 knockdown decreased expression of Nestin (neuronal marker), CD44 (mesenchymal marker), and CD133 (proneural marker), suggesting both miR-194-3p and TAB2 shifts the tumor from a GSC to ML phenotype (Figure S4A). The induced expression miR-194-3p or silencing TAB2 resulted in the cellular phenotypic shift from neurosphere to differentiated. This differentiation effect decreases the expression of GSC genes associated with neurosphere subtype to a modest level. Therefore, to validate the miR-194-3p and TAB2 mediated PMT we used additional proneural subtype markers such as FUT4, and NCAM1 which are not only expressed in neurosphere phenotype but also differentiated adherent phenotype. Proneural gene expression levels in isogenic OSU53 cells supports the PMT shift (Figure S4B). Additionally, exogenous expression of miR-194-3p in PKAC17 exhibited a significant increased expression of Olig2, Sox2 and NCAM1 and a modest decrease in the expression of CD44 (Figure S4C) further substantiates the PMT phenotype switch.

TAB2 promotes radiation resistance and tumorigenicity

NF-κB is known to promote resistance to radiation treatment in GBM.³¹ Therefore, we asked whether TAB2 expression changed the radiosensitization of GBM cells. Validation of TAB2 silencing was confirmed by both TAB2 and NF-κB expression levels in the OSU2 and T98G isogenic cells (Figure 7A). In all the cell lines tested, TAB2 mediated activation or inhibition of NF-κB is universal despite of different mutational landscape of GBMs. Clonogenic survival assay exhibited a radiosensitizing effect with a radiation enhancement ratio of 1.27 in U87-shTAB2,

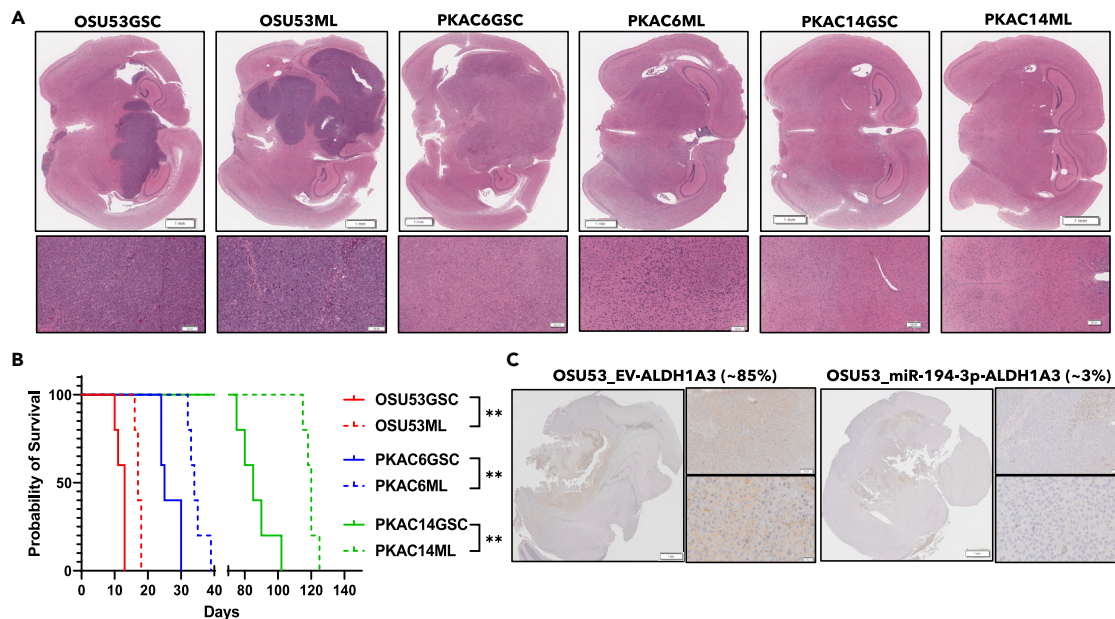


Figure 6. H&E and IHC staining of tumors from P/M subtype, survival of nude mice bearing intracranial tumors

(A) H&E staining of coronal sections of intracranial tumors formed by matched pair ML and GSC cell lines.
 (B) Kaplan-Meier survival curves of matched GSC and ML pairs. The p value was calculated using the two-sided log rank test.
 (C) IHC staining of ALDH1A3 in coronal sections of tumors obtained from nude mice bearing isogenic miR-194-3p cells.

1.6 in OSU2-shTAB2 and 2.0 in T98G-shTAB2 (Figures 7B–7D). This suggests that TAB2 influences the radiosensitization of GBM cells through NF- κ B regulation. To determine whether TAB2 expression impacts the tumorigenicity of GBM cells we conducted intracranial implantation of shTAB2 and NT cells into nude mice. We observed a significant survival benefit of mice bearing shTAB2 tumors (Figure 7E). H&E-stained sagittal sections of NT and shTAB2 clearly shows a considerable reduction in not only the tumor size but also the aggressive nature of the tumor (Figure 7F). Figure 7G summarizes the study as a graphical abstract.

DISCUSSION

We are reporting the GBM biology that includes both neurosphere or GSC and adherent monolayer (ML) phenotype biology. One can obtain both ML and GSC phenotype directly from tumor or differentiate GSC by culturing under serum conditions often referred to as differentiated glioma cells (DGC). Our work focuses on the cellular plasticity of glioma shifting between GSC to ML phenotype. Based on our experience, the differentiation from GSC to ML or dedifferentiation from ML to GSC phenotype is reversible in cells obtained from more than half of the GBM tissues and they can be continuously propagated for more than 10 passages. Serum conditions enriches ML phenotype whereas growth factor defined serum free conditions populate GSC phenotype.

In GBM, the constitutive activation of NF- κ B is demonstrated to promote stem-like properties, enrich the mesenchymal phenotype, and drive treatment-resistance.³⁶ Previous reports have shown that lncRNA, extracellular vesicles, and several gene target activating NF- κ B signaling axis mediating mesenchymal transition.^{34,37–42} Despite the critical role of NF- κ B in dictating GBM cellular identity,²⁹ the key determinants of NF- κ B activity remain poorly understood. Here, we determine that miRNA-194-3p suppresses the activity of NF- κ B during GSC differentiation to their monolayer phenotype, corresponding with a significant suppression of iPSC gene expression. Mechanistically, we determine that miRNA-194-3p targeting of TAB2 disrupts NF- κ B activation. In accordance with our observation, previous reports support the necessity of TAB2 for NF- κ B activity.^{43–46} We demonstrate that the loss of NF- κ B activity results in the decreased activation and/or expression of the oncogenic proteins STAT3 and IL-6. In addition, we determined that miRNA-194-3p regulates the mesenchymal transcriptional subtype of GSCs, demonstrating that miRNA-194-3p regulates stemness in two independent models. TAB2 silencing mimicked the phenotypic, signaling and iPSC gene expression changes induced by miRNA-194-3p expression, confirming that the activity of miRNA-194-3p is primarily dependent on TAB2. In hepatocellular carcinoma, the miRNA-194-3p counterpart miRNA-194-5p is demonstrated to inhibit NF- κ B activity by targeting C21ORF91 and TRIM23.²⁴ In our system, miRNA-194-3p expression did not suppress the expression of C21ORF91 and TRIM23, suggesting that miRNA-194 possesses different context-dependent modes of NF- κ B inhibition.

For the first time, we report the role of miRNA-194-3p dependent inhibition of NF- κ B as a key determinant of transcriptional subtype in GBM. GBM tumors possess inter- and intra-tumoral transcriptomic heterogeneity predominantly comprised of two subtypes mesenchymal (M) and proneural (P).^{47–49} The P and M subtypes exist on a single axis of variation where M correlates with more aggressive tumors and worse prognosis.^{50,51} Genetic tracing of GBM states revealed that the P subtype is supported by intrinsic signaling, whereas the M subtype is largely

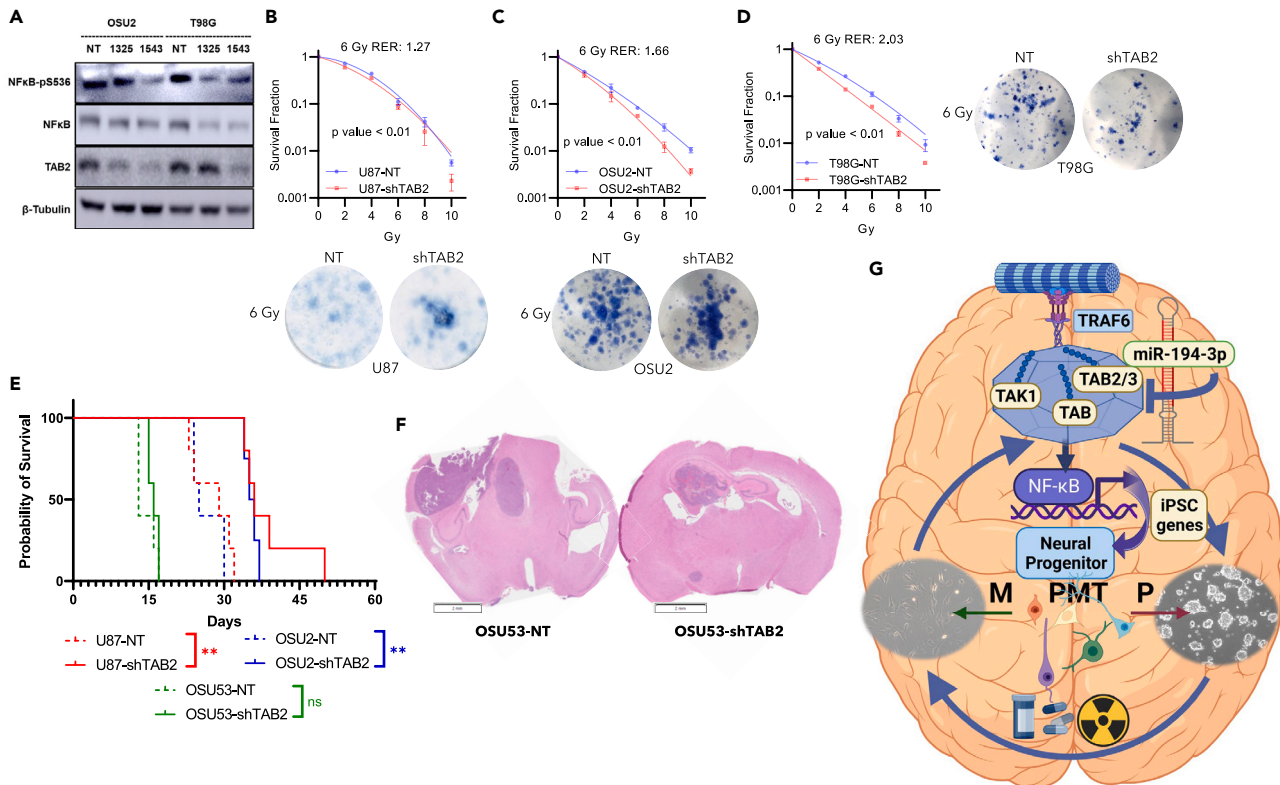


Figure 7. TAB2 silencing enhances radiation sensitivity and prolongs survival of nude mice bearing intracranial tumors and graphical summary

(A) Protein expression levels of TAB2 and NF- κ B activation in T98G and OSU2 cell lines transduced with shTAB2. (B–D) Clonogenic assay comparing the radiosensitivity of NT and shTAB2 cell lines. Cells were fixed and stained 14 days following radiation. Data are shown as mean \pm SEM. Statistical significance was tested using two-tailed unpaired t-test comparing the 6 Gy RER values of shTAB2 to NT in each cell line. The p value for each cell line was less than 0.01. (E) Kaplan-Meier curves demonstrating the survival of mice following intracranial implantation of U87-, OSU2-, and OSU53-shTAB2 isogenic cell lines. The p value was calculated using the two-sided log rank test. (F) H&E-stained coronal sections of tumors from nude mice bearing OSU53-shTAB2 isogenic cells. (G) Schematic summary representing the role of miR-194-3p in regulating PMT by inhibiting TAB2 and NF- κ B activity. ns not significant; **p < 0.01.

adaptive, reversible and builds on a preexisting identity.⁵² P tumors tend to shift to the M subtype following radiation and chemotherapy treatment.^{53–55} The phenotypic plasticity of GBMs is demonstrated to drive treatment resistance to standard-of-care and single-agent targeted therapies.⁵⁶ Therefore, restricting the transcriptional subtype of GBMs offers an exciting opportunity to enhance treatment efficacy.

Altogether, we provide an epigenetic rationale for how GBMs maintain the co-existence of morphologically and epigenetically divergent sub clonal populations within the same tumor. We identify the miRNA-194-3p/TAB2/NF- κ B signaling axis as a previously unknown switch regulating both iPSC gene expression and PMT in GBM. These findings provide critical insight into the underlying mechanisms by which GBMs facilitate the heterogeneous plasticity that drives therapy-tolerant subtypes in response to fluctuating tumor microenvironment and therapeutic selection pressures. Therefore, therapeutic targeting of miRNA-194-3p/TAB2/NF- κ B signaling represents a feasible strategy to restrict phenotype plasticity, decrease GBM stemness, and potentially increase the efficacy of treatment in GBM.

This work focused on GSCs within the proneural and mesenchymal transcriptional subtypes as NF- κ B is reported to promote the shift to from proneural to mesenchymal subtypes. However, we did not assess whether the miR-194-3p/TAB2/NF- κ B signaling axis influences the classical and neural subtypes. The changes in the expression of miR-194-3p did not correlate with the levels of the pre-miR-194-1 or -194-2. This suggests that increased miR-194-3p expression may result from a currently unknown regulatory mechanism (i.e., alternative splicing), which was outside the scope of this work.

Going forward, it will be important to elucidate additional determinants of the transcriptional subtypes in GBM. This insight is essential for the development of therapeutic strategies that aim to limit transcriptional heterogeneity. In this study, GSC transcriptional phenotypes were measured at a population level. Future studies should incorporate a single-cell approach to provide further insight into the role of miR-194-3p, TAB2, and NF- κ B in regulating transcriptional subtype plasticity within GSC cultures and xenograft tumors. Lastly, the identification of transcriptional subtype dependencies represents a promising strategy to develop GBM-specific therapies and limit GBM heterogeneity by depleting specific subtypes.

Limitations of the study

It is becoming better understood through single cell RNA sequencing that heterogeneous GBM tumor has certain proportion of proneural, neural, classical, mixed, mesenchymal transcriptomic subtypes. This work focused on GSCs within the proneural and mesenchymal transcriptional subtypes as NF- κ B promotes the shift to from proneural to mesenchymal subtypes. However, we did not assess whether the miR-194-3p/TAB2/NF- κ B signaling axis influences the classical and neural subtypes. The expression of miR-194-3p did not correlate with the levels of the pre-miR-194-1 or -194-2. This suggests that increased miR-194-3p expression may result from a currently unknown regulatory mechanism.

STAR★METHODS

Detailed methods are provided in the online version of this paper and include the following:

- **KEY RESOURCES TABLE**
- **RESOURCE AVAILABILITY**
 - Lead contact
 - Materials availability
 - Data and code availability
- **EXPERIMENTAL MODEL AND STUDY PARTICIPANT DETAILS**
- **METHOD DETAILS**
 - Cell culture
 - Taqman low density array (TLDA) miRNA profiling and analysis
 - Isogenic cell lines
 - Western analysis
 - Quantitative RT-PCR
 - Clonogenic survival assay
 - Sphere-forming assay
 - Viability assay
 - miRNA reporter assay
 - Intracranial tumor implantation and H&E staining of coronal and sagittal sections
 - NF- κ B activity assay
- **QUANTIFICATION AND STATISTICAL ANALYSIS**

SUPPLEMENTAL INFORMATION

Supplemental information can be found online at <https://doi.org/10.1016/j.isci.2023.108650>.

ACKNOWLEDGMENTS

We thank the patients enrolled in the study and provided biopsies to conduct the study and core facility shared resources at The Ohio State University Comprehensive Cancer Center for sample processing and analysis. This work was supported by grants from NIH/NCI 5R01CA188228, 5UG1CA233331, and The Ohio State University Comprehensive Cancer Center.

AUTHOR CONTRIBUTIONS

K.P. – Project design, coordination, preliminary data collection, hypothesis generation, data analysis, cell culture and *in vivo* study, manuscript reviewing and editing; J.R.J. – Conducted cell culture, luciferase reporter assay, RTqPCR data collection, NF- κ B activity assay, data analysis, and manuscript draft; R.S., M.V., Y.T., and M.O. – Conducted cell culture, RTqPCR and western analysis; A.C. – Provided resources including clinical specimens and data analysis. All authors reviewed and approved the manuscript for publication.

DECLARATION OF INTERESTS

The authors declare no potential conflicts of interests.

INCLUSION AND DIVERSITY

We support inclusive, diverse, and equitable conduct of research.

Received: December 22, 2022

Revised: April 1, 2023

Accepted: December 4, 2023

Published: December 7, 2023

REFERENCES

- Aum, D.J., Kim, D.H., Beaumont, T.L., Leuthardt, E.C., Dunn, G.P., and Kim, A.H. (2014). Molecular and cellular heterogeneity: the hallmark of glioblastoma. *Neurosurg. Focus* 37, E11.
- Palanichamy, K., Jacob, J.R., Litzenberg, K.T., Ray-Chaudhury, A., and Chakravarti, A. (2018). Cells isolated from residual intracranial tumors after treatment express iPSC genes and possess neural lineage differentiation plasticity. *EBioMedicine* 36, 281–292.
- Dirkse, A., Golebiewska, A., Buder, T., Nazarov, P.V., Muller, A., Poovathingal, S., Brons, N.H.C., Leite, S., Sauvageot, N., Sarkisjan, D., et al. (2019). Stem cell-associated heterogeneity in Glioblastoma results from intrinsic tumor plasticity shaped by the microenvironment. *Nat. Commun.* 10, 1787.
- Huber, M.A., Azoitei, N., Baumann, B., Grünert, S., Sommer, A., Pehamberger, H., Kraut, N., Beug, H., and Wirth, T. (2004). NF-kappaB is essential for epithelial-mesenchymal transition and metastasis in a model of breast cancer progression. *J. Clin. Invest.* 114, 569–581.
- Wu, Y., and Zhou, B.P. (2010). TNF-alpha/NF-kappaB/Snail pathway in cancer cell migration and invasion. *Br. J. Cancer* 102, 639–644.
- Tabruyn, S.P., and Griffioen, A.W. (2008). NF-kappa B: a new player in angiostatic therapy. *Angiogenesis* 11, 101–106.
- Liu, T., Zhang, L., Joo, D., and Sun, S.C. (2017). NF-kappaB signaling in inflammation. *Signal Transduct. Target. Ther.* 2, 17023.
- Yu, X., Wang, M., Zuo, J., Wahafu, A., Mao, P., Li, R., Wu, W., Xie, W., and Wang, J. (2019). Nuclear factor I A promotes temozolomide resistance in glioblastoma via activation of nuclear factor kappaB pathway. *Life Sci.* 236, 116917.
- Kim, S.H., Ezhilarasan, R., Phillips, E., Gallego-Perez, D., Sparks, A., Taylor, D., Ladner, K., Furuta, T., Sabit, H., Chhipa, R., et al. (2016). Serine/Threonine Kinase MLK4 Determines Mesenchymal Identity in Glioma Stem Cells in an NF-kappaB-dependent Manner. *Cancer Cell* 29, 201–213.
- Teng, J., da Hora, C.C., Kantar, R.S., Nakano, I., Wakimoto, H., Batchelor, T.T., Chiocca, E.A., Badr, C.E., and Tannous, B.A. (2017). Dissecting inherent intratumor heterogeneity in patient-derived glioblastoma culture models. *Neuro Oncol.* 19, 820–832.
- Anderson, J.D., Johansson, H.J., Graham, C.S., Vesterlund, M., Pham, M.T., Bramlett, C.S., Montgomery, E.N., Mellema, M.S., Bardini, R.L., Contreras, Z., et al. (2016). Comprehensive Proteomic Analysis of Mesenchymal Stem Cell Exosomes Reveals Modulation of Angiogenesis via Nuclear Factor-KappaB Signaling. *Stem Cell.* 34, 601–613.
- Westhoff, M.A., Zhou, S., Nonnenmacher, L., Karpel-Massler, G., Jennewein, C., Schneider, M., Halatsch, M.E., Carragher, N.O., Baumann, B., Krause, A., et al. (2013). Inhibition of NF-kappaB signaling ablates the invasive phenotype of glioblastoma. *Mol. Cancer Res.* 11, 1611–1623.
- Zeligs, K.P., Neuman, M.K., and Annunziata, C.M. (2016). Molecular Pathways: The Balance between Cancer and the Immune System Challenges the Therapeutic Specificity of Targeting Nuclear Factor-kappaB Signaling for Cancer Treatment. *Clin. Cancer Res.* 22, 4302–4308.
- Bennett, J., Capece, D., Begalli, F., Verzella, D., D'Andrea, D., Tornatore, L., and Franzoso, G. (2018). NF-kappaB in the crosshairs: Rethinking an old riddle. *Int. J. Biochem. Cell Biol.* 95, 108–112.
- Lee, J., Kotliarova, S., Kotliarov, Y., Li, A., Su, Q., Donin, N.M., Pastorino, S., Purov, B.W., Christopher, N., Zhang, W., et al. (2006). Tumor stem cells derived from glioblastomas cultured in bFGF and EGF more closely mirror the phenotype and genotype of primary tumors than do serum-cultured cell lines. *Cancer Cell* 9, 391–403.
- Schneider, M., Ströbele, S., Nonnenmacher, L., Siegelin, M.D., Tepper, M., Stroh, S., Hasslacher, S., Enzenmüller, S., Strauss, G., Baumann, B., et al. (2016). A paired comparison between glioblastoma "stem cells" and differentiated cells. *Int. J. Cancer* 138, 1709–1718.
- Tang, J., He, D., Yang, P., He, J., and Zhang, Y. (2018). Genome-wide expression profiling of glioblastoma using a large combined cohort. *Sci. Rep.* 8, 15104.
- Piwecka, M., Rolle, K., Belter, A., Barciszewska, A.M., Żywicki, M., Michalak, M., Nowak, S., Naskręt-Barciszewska, M.Z., and Barciszewski, J. (2015). Comprehensive analysis of microRNA expression profile in malignant glioma tissues. *Mol. Oncol.* 9, 1324–1340.
- Sana, J., Busek, P., Fadrus, P., Besse, A., Radova, L., Vecera, M., Reguli, S., Stollinova Sromova, L., Hilser, M., Lipina, R., et al. (2018). Identification of microRNAs differentially expressed in glioblastoma stem-like cells and their association with patient survival. *Sci. Rep.* 8, 2836.
- Koo, S., Martin, G.S., Schulz, K.J., Ronck, M., and Toussaint, L.G. (2012). Serial selection for invasiveness increases expression of miR-143/miR-145 in glioblastoma cell lines. *BMC Cancer* 12, 143.
- Chen, Y., and Wang, X. (2020). miRDB: an online database for prediction of functional microRNA targets. *Nucleic Acids Res.* 48, D127–D131.
- Liu, W., and Wang, X. (2019). Prediction of functional microRNA targets by integrative modeling of microRNA binding and target expression data. *Genome Biol.* 20, 18.
- Agarwal, V., Bell, G.W., Nam, J.W., and Bartel, D.P. (2015). Predicting effective microRNA target sites in mammalian mRNAs. *Elife* 4, e05005.
- Bao, C., Li, Y., Huan, L., Zhang, Y., Zhao, F., Wang, Q., Liang, L., Ding, J., Liu, L., Chen, T., et al. (2015). NF-kappaB signaling relieves negative regulation by miR-194 in hepatocellular carcinoma by suppressing the transcription factor HNF-1alpha. *Sci. Signal.* 8, ra75.
- Ajibade, A.A., Wang, H.Y., and Wang, R.F. (2013). Cell type-specific function of TAK1 in innate immune signaling. *Trends Immunol.* 34, 307–316.
- Sa, J.K., Yoon, Y., Kim, M., Kim, Y., Cho, H.J., Lee, J.K., Kim, G.S., Han, S., Kim, W.J., Shin, Y.J., et al. (2015). In vivo RNAi screen identifies NLK as a negative regulator of mesenchymal activity in glioblastoma. *Oncotarget* 6, 20145–20159.
- de Souza, C.F., Sabedot, T.S., Malta, T.M., Stetson, L., Morozova, O., Sokolov, A., Laird, P.W., Wiznerowicz, M., Iavarone, A., Snyder, J., et al. (2018). A Distinct DNA Methylation Shift in a Subset of Glioma CpG Island Methylator Phenotypes during Tumor Recurrence. *Cell Rep.* 23, 637–651.
- Noushmehr, H., Weisenberger, D.J., Diefes, K., Phillips, H.S., Pujara, K., Berman, B.P., Pan, F., Pelloski, C.E., Sulman, E.P., Bhat, K.P., et al. (2010). Identification of a CpG island methylator phenotype that defines a distinct subgroup of glioma. *Cancer Cell* 17, 510–522.
- Bhat, K.P.L., Balasubramanian, V., Vaillant, B., Ezhilarasan, R., Hummelink, K., Hollingsworth, F., Wani, K., Heathcock, L., James, J.D., Goodman, L.D., et al. (2013). Mesenchymal differentiation mediated by NF-kappaB promotes radiation resistance in glioblastoma. *Cancer Cell* 24, 331–346.
- Hossain, A., Gumin, J., Gao, F., Figueroa, J., Shinjima, N., Takezaki, T., Priebe, W., Villarreal, D., Kang, S.G., Joyce, C., et al. (2015). Mesenchymal Stem Cells Isolated From Human Gliomas Increase Proliferation and Maintain Stemness of Glioma Stem Cells Through the IL-6/gp130/STAT3 Pathway. *Stem Cell.* 33, 2400–2415.
- Wang, H., Lathia, J.D., Wu, Q., Wang, J., Li, Z., Heddleston, J.M., Elyer, C.E., Elderbroom, J., Gallagher, J., Schuschu, J., et al. (2009). Targeting interleukin 6 signaling suppresses glioma stem cell survival and tumor growth. *Stem Cell.* 27, 2393–2404.
- Sherry, M.M., Reeves, A., Wu, J.K., and Cochran, B.H. (2009). STAT3 is required for proliferation and maintenance of multipotency in glioblastoma stem cells. *Stem Cell.* 27, 2383–2392.
- Zhang, G., Tanaka, S., Jiapaer, S., Sabit, H., Tamai, S., Kinoshita, M., and Nakada, M. (2020). RBPJ contributes to the malignancy of glioblastoma and induction of proneural-mesenchymal transition via IL-6-STAT3 pathway. *Cancer Sci.* 111, 4166–4176.
- Schweiger, M.W., Li, M., Giovanazzi, A., Fleming, R.L., Tabet, E.I., Nakano, I., Würdinger, T., Chiocca, E.A., Tian, T., and Tannous, B.A. (2020). Extracellular Vesicles Induce Mesenchymal Transition and Therapeutic Resistance in Glioblastomas through NF-kappaB/STAT3 Signaling. *Adv. Biosyst.* 4, e1900312.
- McFarland, B.C., Hong, S.W., Rajbhandari, R., Twitty, G.B., Jr., Gray, G.K., Yu, H., Benveniste, E.N., and Nozell, S.E. (2013). NF-kappaB-induced IL-6 ensures STAT3 activation and tumor aggressiveness in glioblastoma. *PLoS One* 8, e78728.
- Garner, J.M., Fan, M., Yang, C.H., Du, Z., Sims, M., Davidoff, A.M., and Pfeffer, L.M. (2013). Constitutive activation of signal transducer and activator of transcription 3 (STAT3) and nuclear factor kappaB signaling in glioblastoma cancer stem cells regulates the Notch pathway. *J. Biol. Chem.* 288, 26167–26176.
- Liang, Q., Guan, G., Li, X., Wei, C., Wu, J., Cheng, P., Wu, A., and Cheng, W. (2020). Profiling pro-neural to mesenchymal transition identifies a lncRNA signature in glioma. *J. Transl. Med.* 18, 378.
- Chen, Z., Wang, S., Li, H.L., Luo, H., Wu, X., Lu, J., Wang, H.W., Chen, Y., Chen, D., Wu, W.T., et al. (2022). FOSL1 promotes proneural-to-mesenchymal transition of glioblastoma stem cells via UBC9/CYLD/NF-kappaB axis. *Mol. Ther.* 30, 2568–2583.
- Zhang, Z., Xu, J., Chen, Z., Wang, H., Xue, H., Yang, C., Guo, Q., Qi, Y., Guo, X., Qian, M.,

- et al. (2020). Transfer of MicroRNA via Macrophage-Derived Extracellular Vesicles Promotes Proneural-to-Mesenchymal Transition in Glioma Stem Cells. *Cancer Immunol. Res.* 8, 966–981.
40. Tang, G., Luo, L., Zhang, J., Zhai, D., Huang, D., Yin, J., Zhou, Q., Zhang, Q., and Zheng, G. (2021). lncRNA LINC01057 promotes mesenchymal differentiation by activating NF- κ B signaling in glioblastoma. *Cancer Lett.* 498, 152–164.
 41. Wang, H., Li, L., and Yin, L. (2018). Silencing lncRNA LOXL1-AS1 attenuates mesenchymal characteristics of glioblastoma via NF- κ B pathway. *Biochem. Biophys. Res. Commun.* 500, 518–524.
 42. Qin, J., Jiang, C., Cai, J., and Meng, X. (2021). Roles of Long Noncoding RNAs in Conferring Glioma Progression and Treatment. *Front. Oncol.* 11, 688027.
 43. Suzuki, S., Singhirunnusorn, P., Mori, A., Yamaoka, S., Kitajima, I., Saiki, I., and Sakurai, H. (2007). Constitutive activation of TAK1 by HTLV-1 tax-dependent overexpression of TAB2 induces activation of JNK-ATF2 but not IKK-NF- κ B. *J. Biol. Chem.* 282, 25177–25181.
 44. Qiu, H., Huang, F., Xiao, H., Sun, B., and Yang, R. (2013). TRIM22 inhibits the TRAF6-stimulated NF- κ B pathway by targeting TAB2 for degradation. *Viroi. Sin.* 28, 209–215.
 45. Tan, B., Mu, R., Chang, Y., Wang, Y.B., Wu, M., Tu, H.Q., Zhang, Y.C., Guo, S.S., Qin, X.H., Li, T., et al. (2015). RNF4 negatively regulates NF- κ B signaling by down-regulating TAB2. *FEBS Lett.* 589, 2850–2858.
 46. Kanayama, A., Seth, R.B., Sun, L., Ea, C.K., Hong, M., Shaito, A., Chiu, Y.H., Deng, L., and Chen, Z.J. (2004). TAB2 and TAB3 activate the NF- κ B pathway through binding to polyubiquitin chains. *Mol. Cell* 15, 535–548.
 47. Verhaak, R.G.W., Hoadley, K.A., Purdom, E., Wang, V., Qi, Y., Wilkerson, M.D., Miller, C.R., Ding, L., Golub, T., Mesirov, J.P., et al. (2010). Integrated genomic analysis identifies clinically relevant subtypes of glioblastoma characterized by abnormalities in PDGFRA, IDH1, EGFR, and NF1. *Cancer Cell* 17, 98–110.
 48. Lee, J.K., Wang, J., Sa, J.K., Ladewig, E., Lee, H.O., Lee, I.H., Kang, H.J., Rosenbloom, D.S., Camara, P.G., Liu, Z., et al. (2017). Spatiotemporal genomic architecture informs precision oncology in glioblastoma. *Nat. Genet.* 49, 594–599.
 49. Sottoriva, A., Spiteri, I., Piccirillo, S.G.M., Touloumis, A., Collins, V.P., Marioni, J.C., Curtis, C., Watts, C., and Tavaré, S. (2013). Intratumor heterogeneity in human glioblastoma reflects cancer evolutionary dynamics. *Proc. Natl. Acad. Sci. USA* 110, 4009–4014.
 50. Colman, H., Zhang, L., Sulman, E.P., McDonald, J.M., Shooshtari, N.L., Rivera, A., Popoff, S., Nutt, C.L., Louis, D.N., Cairncross, J.G., et al. (2010). A multigene predictor of outcome in glioblastoma. *Neuro Oncol.* 12, 49–57.
 51. Wang, L., Babikir, H., Müller, S., Yagnik, G., Shamardani, K., Catalan, F., Kohanbash, G., Alvarado, B., Di Lullo, E., Kriegstein, A., et al. (2019). The Phenotypes of Proliferating Glioblastoma Cells Reside on a Single Axis of Variation. *Cancer Discov.* 9, 1708–1719.
 52. Schmitt, M.J., Company, C., Dramaretska, Y., Barozzi, I., Göhrig, A., Kertalli, S., Großmann, M., Naumann, H., Sanchez-Bailon, M.P., Hulsman, D., et al. (2021). Phenotypic Mapping of Pathologic Cross-Talk between Glioblastoma and Innate Immune Cells by Synthetic Genetic Tracing. *Cancer Discov.* 11, 754–777.
 53. Segerman, A., Niklasson, M., Haglund, C., Bergström, T., Jarvius, M., Xie, Y., Westermark, A., Sönmez, D., Hermansson, A., Kastemar, M., et al. (2016). Clonal Variation in Drug and Radiation Response among Glioma-Initiating Cells Is Linked to Proneural-Mesenchymal Transition. *Cell Rep.* 17, 2994–3009.
 54. Halliday, J., Helmy, K., Pattwell, S.S., Pitter, K.L., LaPlant, Q., Ozawa, T., and Holland, E.C. (2014). In vivo radiation response of proneural glioma characterized by protective p53 transcriptional program and proneural-mesenchymal shift. *Proc. Natl. Acad. Sci. USA* 111, 5248–5253.
 55. Phillips, H.S., Kharbanda, S., Chen, R., Forrest, W.F., Soriano, R.H., Wu, T.D., Misra, A., Nigro, J.M., Colman, H., Soroceanu, L., et al. (2006). Molecular subclasses of high-grade glioma predict prognosis, delineate a pattern of disease progression, and resemble stages in neurogenesis. *Cancer Cell* 9, 157–173.
 56. Meyer, M., Reimand, J., Lan, X., Head, R., Zhu, X., Kushida, M., Bayani, J., Pressey, J.C., Lionel, A.C., Clarke, I.D., et al. (2015). Single cell-derived clonal analysis of human glioblastoma links functional and genomic heterogeneity. *Proc. Natl. Acad. Sci. USA* 112, 851–856.
 57. Palanichamy, K., Kanji, S., Gordon, N., Thirumoorthy, K., Jacob, J.R., Litzenberg, K.T., Patel, D., and Chakravarti, A. (2017). NNMT Silencing Activates Tumor Suppressor PP2A, Inactivates Oncogenic STKs, and Inhibits Tumor Forming Ability. *Clin. Cancer Res.* 23, 2325–2334.

STAR★METHODS

KEY RESOURCES TABLE

REAGENT or RESOURCE	SOURCE	IDENTIFIER
<i>Antibodies</i>		
β-Actin	CST	Cat#3799; RRID:AB_2242334
Axin	CST	Cat#2087; RRID:AB_2274550
β-catenin	CST	Cat#8480; RRID:AB_11127855
phospho-β-catenin	CST	Cat#9561; RRID:AB_331729
CD44	CST	Cat#37529; RRID:AB_2750879
Cyclin D1	CST	Cat#2922; RRID: AB_2228523
GSK3β	CST	Cat#12456; RRID:AB_2636978
IL6	CST	Cat#12153; RRID: AB_2687897
LRP6	CST	Cat#3395; RRID: AB_1950408
phospho-LRP6	CST	Cat#2568; RRID: AB_2139327
Mouse IgG–HRP	CST	Cat#7076; RRID:AB_330924
c-Myc	CST	Cat#18583; RRID:AB_2895543
Nanog	CST	Cat#8822; RRID:AB_11217637
NFκB	CST	Cat#8242; RRID:AB_10859369
phospho-NFκB (S536)	CST	Cat#3033; RRID:AB_331284
NLK	CST	Cat#94350; RRID:AB_2800227
OCT4	CST	Cat# 2750; RRID: AB_823583
STAT3	CST	Cat#12640; RRID:AB_2629499
phospho-STAT3 (Y705)	CST	Cat#9131; RRID:AB_331586
Rabbit IgG–HRP	CST	Cat#2729; RRID:AB_1031062
TAB2	CST	Cat#3745; RRID: AB_2297368
TAK1	CST	Cat# 4505; RRID:AB_490858
phospho-TAK1 (T184)	Thermo Fisher	Cat#MA5-15073; RRID:AB_10982333
TCF1/7	CST	Cat#2203; RRID_2797631
β-tubulin	CST	Cat#2146; RRID:AB_2210545
WLS	Novus Biologicals	Cat#NBP-57299
<i>Chemicals, peptides, and recombinant proteins</i>		
DMEM	Life Technologies	Cat#11965118
DMEM F12	Life Technologies	Cat#11320033
FBS	VWR	Cat#97068-107
B27	Gibco	Cat#17504044
100x Antibiotic-Antimycotic	Life Technologies	Cat#15240096
EGF	Thermo Fischer	Cat#PHG0313
FGF	Thermo Fischer	Cat#PHG0368
Puromycin	Sigma	Cat#P9620
RIPA buffer	Sigma	Cat#R0278
Protease inhibitor cocktail	Sigma	Cat#P8340
Phosphatase inhibitor cocktail	Sigma	Cat#P0044
XbaI	NEB	Cat#R0145T
EagI-HF	NEB	Cat#R3505L
T4 ligase	NEB	Cat#M0202S

(Continued on next page)

Continued

REAGENT or RESOURCE	SOURCE	IDENTIFIER
Lipofectamine 3000	Thermo Fischer	Cat#L3000015
MISSION® siRNA Transfection Reagent	Sigma	Cat#S1452
Epitope retrieval TRIS pH 6.1	Agilent	Cat#S236984-2

Critical commercial assays

TaqMan Array MicroRNA Cards	Applied Biosystems	Cat#4444913
Megaplex RT primers	Applied Biosystems	Cat#4399966
Megaplex Pre-amp primers	Applied Biosystems	Cat#4444748
RNeasy Mini Kit	Qiagen	Cat#74104
Superscript III First-Strand Synthesis Kit	Thermo Fisher	Cat#18080051
mirVana miRNA Isolation Kit	Thermo Fisher	Cat#AM1560
TaqMan™ Advanced miRNA cDNA Synthesis Kit	Thermo Fisher	Cat#A28007
MTT Assay Kit	abcam	Cat#ab113474
Nuclear Extraction Kit	abcam	Cat#ab113474
NF-κB p65 Transcription Factor Assay Kit	abcam	Cat#ab133112
pMIR-REPORT™ miRNA Expression Reporter Vector System	Thermo Fisher	Cat#AM5795
Dual-Luciferase® Reporter Assay System	Promega	Cat#E1910
H&E Staining Kit	abcam	Cat#ab245880

Experimental models: Cell lines

A172	ATCC	Cat# CRL-1620; RRID:CVCL_0131
LN229	ATCC	Cat# CRL-2611; RRID:CVCL_0393
T98G	ATCC	Cat#CRL-1690; RRID:CVCL_0556
U87	ATCC	Cat#HTB-14; RRID:CVCL_0022

Experimental models: Organisms/strains

Nude mice (NU/J)	The Jackson Laboratory	RRID:IMSR_JAX:002019
------------------	------------------------	----------------------

Oligonucleotides and RTQPCR Probes

194-1	Thermo Fisher	Cat#Hs04231530_s1
194-2	Thermo Fisher	Cat#Hs04331541_s1
ALDH1A3	Thermo Fisher	Cat#Hs00167476_m1
C21orf91	Thermo Fisher	Cat#Hs05040994_s1
CD133	Thermo Fisher	Cat#Hs01009259_m1
CD44	Thermo Fisher	Cat#Hs05662929_s1
CMYC	Thermo Fisher	Cat#Hs00153408_m1
DOCK5	Thermo Fisher	Cat#Hs07287975_m1
FAS	Thermo Fisher	Cat#Hs00236330_m1
FUT4	Thermo Fisher	Cat#Hs01106466_s1
GAPDH	Thermo Fisher	Cat#Hs99999905_m1
HFE	Thermo Fisher	Cat#Hs00373474_m1
KLF4	Thermo Fisher	Cat#Hs00358836_m1
LGALS3	Thermo Fisher	Cat#Hs07288627_m1
LYN	Thermo Fisher	Cat#Hs01015818_g1
MAL	Thermo Fisher	Cat#Hs00707014_s1
NANOG	Thermo Fisher	Cat#Hs02387400_g1
NCAM1	Thermo Fisher	Cat#Hs00941830_m1
NESTIN	Thermo Fisher	Cat#Hs04187831_g1

(Continued on next page)

Continued

REAGENT or RESOURCE	SOURCE	IDENTIFIER
OLIG1	Thermo Fisher	Cat#Hs00907227_s1
OCT4	Thermo Fisher	Cat#Hs00999632_g1
RHOF	Thermo Fisher	Cat#Hs00368032_m1
SOWAHA	Thermo Fisher	Cat#Hs00703106_s1
SOX2	Thermo Fisher	Cat#Hs04234836_s1
TAB2	Thermo Fisher	Cat#Hs00248373_m1
TRIM23	Thermo Fisher	Cat#Hs01106626_m1
WT1	Thermo Fisher	Cat#Hs01103751_m1
mir-194-3p	Thermo Fisher	Cat#002379
RNU6B	Thermo Fisher	Cat#001093
has-mir-194-3p mimic	Sigma	Cat#HMI0319
has-mir-194-3p inhibitor	Sigma	Cat#HSTUD0319
has-mir-194-3p lentivirus	Sigma	Cat#HLMIR0319
miRNA negative control lentivirus	Sigma	Cat#NCLMIR001
shTAB2 lentivirus	Sigma	Cat#SHCLNV-NM_015093
Non-target shRNA lentiviral particles	Sigma	SHC016H-1EA

Software and algorithms	RRID
SAS 9.2	RRID: SCR_008567
GraphPad Prism 5	RRID: SCR_002798

RESOURCE AVAILABILITY**Lead contact**

Further information and requests for resources and reagents should be directed to and will be fulfilled by the lead contact, Kamalakannan Palanichamy (Kamalakannan.palanichamy@osumc.edu).

Materials availability

Patient derived glioma stem cells generated are available with [lead contact](#) and can be shared upon requests.

Data and code availability

- Data generated were included in the paper
- This paper does not report original code.
- Any additional information is available from the [lead contact](#) upon request.

EXPERIMENTAL MODEL AND STUDY PARTICIPANT DETAILS

We have used fourteen patient-derived and four commercially available glioblastoma cell lines. We enriched glioma stem cells (GSC) and adherent monolayer (ML) subtypes from patient biopsies. This study was conducted in accordance with The Ohio State University Institutional Review Boards for IRB (2009C0065 and 2014C0115), IACUC (2009A0127), and IBC (2009R0169). Additional details are as follows.

METHOD DETAILS**Cell culture**

Primary glioblastoma cell lines (OSU2, OSU4, OSU11, OSU13, OSU20, OSU30, OSU53, OSU68, OSU82, OSU94, GBM, PKAC6, PKAC14, PKAC17, ACPK4) used in this study were isolated from glioblastoma patient tissues authenticated by neuropathologist and characterized using STR phenotyping of tissues and cell lines (Table S5). The biopsies used in the study are pathologically diagnosed GBM. Tumors obtained from patient biopsies was minced and enzymatically dissociated using Tryple (Invitrogen) and mechanically dissociated using a G20 10 mL syringe to obtain a cell suspension. The cell suspension was passed through cell strainer (BD) to obtain a single cell suspension. Neurosphere initiation medium was added to the cells consisting of the following: DMEM-F12 (GIBCO) medium, B27 supplement (GIBCO), human-basic fibroblast growth factor (20 ng/mL) (Invitrogen), human-epidermal growth factor (20 ng/mL) (Invitrogen), penicillin/streptomycin (100 U/mL) (GIBCO), and Amphotericin B (5 ng/mL) (Sigma). Cultures were fed every two days until they reach confluency. Cultures were passaged every

week by collecting the floating spheres by centrifugation at 1000 rpm for 5 min at 4°C. The spent media was aspirated and the pellet was mechanically dissociated and seeded in fresh medium. The A172, LN229, U87 and T98G cell line was obtained from ATCC (ATCC Cat# CRL-1620, ATCC Cat# CRL-2611, ATCC Cat# HTB-14, ATCC Cat# CRL-1690). All the cell lines were free from mycoplasma contamination. Monolayer glioblastoma cells were maintained in DMEM (Life Technologies: 11965118), supplemented with 10% FBS (VWR: Cat# 97068-107), and 1% antibiotic-antimycotic (Life Technologies: Cat# 15240096). GSC glioblastoma cells were maintained in DMEM F12 (Life Technologies: Cat# 11320033), supplemented with B27 (Gibco: Cat# 17504044), 20 ng/mL EGF (Thermo Fisher: Cat# PHG0313), 20 ng/mL FGF (Thermo Fisher: Cat# PHG0368), and 1% antibiotic-antimycotic (Life Technologies: Cat# 15240096). All cells were cultured at 37°C under a gas phase of 95% air and 5% CO₂. All studies were conducted within 10 passages.

Taqman low density array (TLDA) miRNA profiling and analysis

In the discovery dataset four matched pair of GSC and ML cells were used U87, OSU2, OSU11, and OSU68 cells were used. Comprehensive coverage of Sanger miRBase v14 is enabled across a two-card set of TaqMan Array MicroRNA Cards (Cards A and B) for a total of 754 unique assays specific to human miRNAs (Applied Biosystems: Cat# 4444913). TaqMan Array MicroRNA Cards contains four control assays. Profiling was conducted as per the manufacturer's protocol. Briefly, 10 ng RNA was initially reverse transcribed using Megaplex RT primers (Applied Biosystems: Cat# 4399966) followed by pre-amplification using Megaplex Pre-amp primers (Applied Biosystems: Cat# 4444748). Pre-amplified product was loaded on the miRNA card and run on 7900HT RTqPCR. Data was processed and analyzed using RQ manager by adopting global normalization algorithm. The differentially regulated miRNAs were validated using TaqMan miRNA assays in replicates. The discovery and validation cohorts global normalization and U6 were used respectively. The data was analyzed using t-test and Bonferroni correction for false positives. A $p < 0.05$ was considered statistically significant.

Isogenic cell lines

U87, OSU53, and PKAC17 cells were transduced with the has-mir-194-3p overexpression lentivirus (Sigma: Cat# HLMIR0319) and miRNA negative control lentivirus (Sigma: Cat# NCLMIR001). U87, T98G, and OSU2 cells were transduced with lentiviral particles (Sigma: Cat# SHCLNV-NM_015093) containing the shTAB2 constructs. Non-target shRNA lentiviral particles (Sigma: Cat# SHC016H-1EA) were transduced as a negative control. Transduced cells were selected with puromycin (10 ng/mL) (Sigma: Cat# P9620) for 5 days and gene silencing was validated through qRT-PCR and Western blot.

shTAB2 constructs with target sequence as indicated:

236: (CCGGCCTGAAGTACCTGAAGTTGTTCTCGAGAACAACCTTCAGGTACTTCAGGTTTTT),
 1325: (CCGGAGTCAACCTAAGGTCTATATTCTCGAGAATATAGACCTTAGGTTGACTTTTTG),
 1543: (CCGGCACTCAGCCCAATACGAAATACTCGAGTATTCGTATTGGGCTGAGTGTTTTTG),
 1983: (CCGGAGATTGACATTGACTGCTTAACTCGAGTTAAGCAGTCAATGTCAATCTTTTTT),
 2214: (CCGGTGGCCCTGTATCTTCTCTAACTCGAGTTTAGAGAAGATACAGGGCCATTTTTT).

Non-target shRNA lentiviral particles (Sigma: Cat# SHC016H-1EA) were transduced as a negative control. Transduced cells were selected with puromycin (10 ng/mL) (Sigma: Cat# P9620) for 5 days and gene silencing was validated through qRT-PCR and Western blot.

Western analysis

Cells were harvested and protein was extracted using RIPA buffer (Sigma: Cat# R0278) with 1% (v/v) protease inhibitor cocktail (Sigma: Cat# P8340) and 1% (v/v) phosphatase inhibitor cocktail (Sigma: Cat# P0044). Samples were run on SDS-PAGE gels and transferred to PVDF membranes. The membranes were then incubated overnight with the following primary antibodies followed by incubation for 1 h with mouse or rabbit IgG-HRP conjugate secondary antibodies (CST: Cat# 2729 & 7076) and developed.

The membranes were then incubated overnight with the following primary antibodies: WLS (Novus Biologicals: Cat# NBP-57299), phospho-LRP6 (R&D: Cat# S1490) (CST: Cat# 2568), LRP6 (CST: Cat# 3395), Axin (CST: Cat# 2087), GSK3β (CST: Cat# 12456), Cyclin D1 (CST: Cat# 55506), TCF1/7 (CST: Cat# 2203), phospho-β-catenin (S33/S37/T31) (CST: Cat# 9561), β-catenin (CST: Cat# 8480), β-Actin (CST: Cat# 3700), NLK (CST: Cat# 94350), CD44 (CST: Cat# 37259), c-Myc (CST: Cat# 18583), TAB2 (CST: Cat# 3745), NF-κB (CST: Cat# 8242), phospho-NFκB (S536) (CST: Cat# 3033), OCT4 (CST: Cat# 2750), Nanog (CST: Cat# 8822), phospho-STAT3 (Y705) (CST: Cat# 9145), STAT3 (CST: Cat# 12640), phospho-TAK1 (T184) (Thermo Fisher: Cat# MA5-15073), TAK1 (CST: Cat# 5206), IL6 (CST: Cat# 12153), and β-tubulin (CST: Cat# 2146). The membranes were then incubated for 1 h with mouse or rabbit IgG-HRP conjugate secondary antibodies (CST: Cat# 2729 & 7076) and developed.

Quantitative RT-PCR

The RNeasy Mini Kit (Qiagen: Cat# 74104) and Superscript III First-Strand Synthesis Kit (Thermo Fisher: Cat# 18080051) were used to isolate RNA from samples and generate cDNA according to the manufacturer's instructions. Taqman gene expression assay probes were used to measure the premir, miRNA, and mRNA levels. Taqman gene expression assay probes were used to measure the mRNA levels of 194-1 (Thermo Fisher: Cat# Hs04231530_s1), 194-2 (Thermo Fisher: Cat# Hs04331541_s1), ALDH1A3 (Thermo Fisher: Cat# Hs00167476_m1), CD44 (Thermo Fisher: Cat# Hs05662929_s1), LYN (Thermo Fisher: Cat# Hs01015818_g1), WT1 (Thermo Fisher: Cat# Hs01103751_m1), CD133 (Thermo Fisher: Cat# Hs01009259_m1), Nestin (Thermo Fisher: Cat# Hs04187831_g1), OLIG1 (Thermo Fisher: Cat# Hs00907227_s1),

SOX2 (Thermo Fisher: Cat# Hs04234836_s1), klf4 (Thermo Fisher: Cat# Hs00358836_m1), OCT4 (Thermo Fisher: Cat# Hs00999632_g1), FUT4 (Thermo Fisher: Cat# Hs01106466_s1), NCAM1 (Thermo Fisher: Cat# Hs00941830_m1), Nanog (Thermo Fisher: Cat# Hs02387400_g1), TAB2 (Thermo Fisher: Cat# Hs00248373_m1), CMYC (Thermo Fisher: Cat# Hs00153408_m1), DOCK5 (Thermo Fisher: Cat# Hs07287975_m1), FAS (Thermo Fisher: Cat# Hs00236330_m1), HFE (Thermo Fisher: Cat# Hs00373474_m1), LGALS3 (Thermo Fisher: Cat# Hs07288627_m1), MAL (Thermo Fisher: Cat# Hs00707014_s1), RHOF (Thermo Fisher: Cat# Hs00368032_m1), SOWAHA (Thermo Fisher: Cat# Hs00703106_s1), C21orf91 (Thermo Fisher: Cat# Hs05040994_s1), TRIM23 (Thermo Fisher: Cat# Hs01106626_m1). GAPDH (Thermo Fisher: Cat# Hs99999905_m1) was used as the control. miRNA was isolated using the mirVana miRNA Isolation Kit (Thermo Fisher: Cat# AM1560). Isolated miRNA was converted to cDNA using TaqMan Advanced miRNA cDNA Synthesis Kit (Thermo Fisher: Cat# A28007). Advanced miRNA Taqman probes were used to measure the levels of mir-194-3p (Thermo Fisher: Cat# 002379) and control RNU6B (Thermo Fisher: Cat# 001093). The gene expression profile data were generated using the C1000TM Thermal Cycler-CFX96TM Real-Time System and analyzed using the BIO-RAD CFX Manager.

Clonogenic survival assay

Cells were plated at 8,000, 4,000, 2,000, 1,000, 500, and 50 cells/well in petri dishes and radiated at 10, 8, 6, 4, 2, and 0 Gy, respectively. The plates were incubated in a humidified CO₂ incubator at 37°C and cultured for 10 to 14 days depending on colony size and cell type. After 10 to 14 days, surviving colonies were stained with methylene blue, dried, and counted. Colonies of 50 cells were considered significant. The plating efficiency was calculated from the ratio of colonies formed over the number of cells plated.

Sphere-forming assay

1×10^5 monolayer cells were plated in monolayer growth conditions and incubated for 24 h. Cells were washed twice with PBS and GSC growth media was added to the plates. Ability of cells to detach and form spheres was monitored over a ten day period.

Viability assay

The MTT Assay Kit was used according to the manufacturer's instructions (ATCC: Cat# 30-1010K). Briefly, the proliferation rate was determined by measuring the amount of oxidoreductase enzymes. These enzymes reduce the yellow tetrazolium MTT to generate the insoluble purple product formazan quantified by measuring the absorbance at 570 nm.

miRNA reporter assay

pMIR-REPORT miRNA Expression Reporter Vector System (Thermo Fisher: Cat# AM5795) was used to measure the ability of has-mir-194-3p to target the 3' UTR of TAB2. After a 2 h incubation with appropriate reagents, the Renilla and Firefly luciferase intensities were measured subsequently with the Dual-Luciferase Reporter Assay System (Promega: Cat# E1910). Renilla luciferase intensity was used to normalize the firefly luciferase intensity. An oligo mimicking the 3' UTR of TAB2 (3' UTR TAB2: GGCCCCACTGTAACCCACTGCCACCCACTGGTG) was cloned into the reporter vector system upstream of the firefly luciferase protein. A negative control oligo (3' UTR TAB2 mismatch: GGCAAACAGTTAAAAACAGTCCAAACAGTGTG) was similarly cloned into the reporter system. *Xba*I (NEB: Cat# R0145T) and *Eag*I-HF (NEB: Cat# R3505L) restriction enzymes were used to cleave the pMIR-REPORT miRNA Expression Reporter Vector and oligos. The T4 ligase (NEB: Cat# M0202S) was then used to ligate the oligos into the reporter vector. The TAB2 and mismatch inserts were verified by sanger sequencing to ensure the correct sequence and orientation. About 0.625 µg of each plasmid was transfected into 1×10^4 cells in a 96-well plate using Lipofectamine 3000 (Thermo Fisher: Cat# L3000015). Cells were incubated for 24 h hsa-mir-194-3p mimic (Sigma: HMI0319) and hsa-mir-194-3p inhibitor (Sigma: Cat# HSTUD0319) were added to a final concentration of 100 nM using the MISSION siRNA Transfection Reagent (Sigma: Cat# S1452). After a 2 h incubation, the Renilla and Firefly luciferase intensities were measured subsequently with the Dual-Luciferase Reporter Assay System (Promega: Cat# E1910). Renilla luciferase intensity was used to normalize the firefly luciferase intensity.

Intracranial tumor implantation and H&E staining of coronal and sagittal sections

Three-to four-week-old nude mice were orthotopically implanted with GBM cells. A small anterior-posterior incision through scalp was made down to the level of the bone. The bur hole was made exactly 2 mm from the bregma at the right frontal lobe. Cells in a 3 µL volume of medium were injected intracranially using a stereotactic frame. Tumor formation and tumor burden were evaluated using sequential weight loss, and neurological symptoms such as lethargy, poor feeding, paralysis, appearance of distress such as poor mobility, self-mutilation, hunched posture, dehydrations and skin ulcerations, and weight loss exceeding 20%. Observation of these symptoms resulted in euthanization. The brain was recovered for further processing such as formalin fixation and generating paraffin blocks. Hematoxylin and Eosin (H&E) staining (abcam: ab245880) was conducted to estimate tumor burden. The brain was recovered for further processing such as formalin fixation and generating paraffin blocks. Hematoxylin and Eosin (H&E) staining (abcam: ab245880) was conducted to estimate tumor burden. Formalin-fixed, paraffin embedded tissue sections were baked overnight at 60°C, deparaffinized, rehydrated using xylene and ethanol graded mixture, treated with epitope retrieval agent (Dako-TRS pH 6.1; Agilent: Cat# S236984-2). Sections were stained with hematoxylin for 5 min, rinsed in running tap water and counterstained in Eosin for 15 s, and mounted after dehydration. Thorough washing with PBS (3x) was ensured after all incubation steps. The sample size for intracranial injection was determined based on the power calculation from an *in vivo* experiment

performed previously.⁵⁷ It was determined that five mice would be sufficient to determine an effect size of 5 days with a power of 0.90 and significance level of 0.05. Differences in tumor growth between the different cell lines was determined using a p value of >0.05.

NF- κ B activity assay

2×10^6 cells were plated in a Petri dish and incubated for 24 h. The nuclear fraction was isolated using the Nuclear Extraction Kit (abcam: Cat# ab113474). The isolated nuclear fraction was used to measure the transcriptional activity of NF- κ B with the NF- κ B p65 Transcription Factor Assay Kit (abcam: Cat# ab133112) according to the manufacturer's instructions. 25 μ L of the provided Transcription Factor NF- κ B Competitor dsDNA was used to demonstrate specificity.

QUANTIFICATION AND STATISTICAL ANALYSIS

All results were confirmed in at least three independent experiments, and data from one representative experiment were shown. All quantitative data are presented as mean \pm SD. The statistical analysis was performed using SAS 9.2 or GraphPad Prism 5. Student t tests were used for comparisons of means of quantitative data between groups. Values of $p < 0.05$ were considered significant.